Mode Coupling in Superconducting Parallel Plate Resonator in a Cavity with Outer Conductive Enclosure

Feng Gao, *Member, IEEE*, M. V. Klein, *Senior Member, IEEE*, Jay Kruse, *Member, IEEE*, and Milton Feng, *Fellow, IEEE*

***Abstract*—We have carefully studied the mode coupling effect from analysis of the measured microwave scattering parameters of superconducting films using a parallel-plate-resonator technique. Due to its high resolution and simplicity, this technique has been widely employed to identify the quality of high-T_c superconducting films by measuring the resonance bandwidth, from which the microwave surface resistance is directly derived. To minimize the radiation loss, the resonator is usually housed in a conductive cavity. Using this method, we observe that a number of strong "cavity" modes due to the test enclosure fall around the lowest TM mode of the superconducting resonator and that a strong interaction between these two types of resonant modes occurs when their eigenfrequencies are close, causing a significant distortion or a strong antiresonance for the resonator mode. To describe this effect, a coupled harmonic-oscillator model is proposed. We suggest that the interaction arises from a phase interference or a linear coupling among the individual oscillators. Our model fits very well the observed Fano-type asymmetric or antiresonant features, and thus can be used to extract the intrinsic Q of the superconducting resonator.**

I. Introduction

HIGH temperature superconductors (HTS) have potential commercial applications in microwave devices [1]–[7] due to their extremely low high-frequency loss and small dispersion compared with normal metals at temperatures even above the boiling point (77 K) of liquid nitrogen, a readily available coolant that is much less expensive than liquid helium, which is required for conventional superconductors. The electronic properties of HTS can be exploited for use in a variety of high-performance microelectronic components such as analog and logic circuits, vortex flow transistors, multichip module interconnects, delay lines, filters, and infrared detectors. The fabrication of ultrasensitive sensors and production of Josephson microwave mixers with wider electromagnetic wave windows becomes possible with the use of HTS because of the large expected energy gap for these materials.

To explore the possibilities of these applications, it is essential to investigate the microelectronic mechanisms and to determine accurately some fundamental parameters of high quality superconducting films at microwave frequencies. One key parameter frequently measured is the temperature-dependent complex impedance, $Z_s(T) = R_s + jX_s$, from which the London penetration depth $\lambda_L(T)$, complex conductivity $\sigma(T) = \sigma_1 - j\sigma_2$, superconducting order parameters $\Delta(T)$, and quasiparticle scattering time $\tau(T)$ can be deduced [8].

Microwave surface resistance in principle can be measured in a variety of traditional methods. However, because of the limitation that high-T_c materials are highly anisotropic and of the requirements that the HTS thin films can be grown only on substrates such as sapphire, MgO, $LaAlO_3$, $SrTiO_3$, or yttria-stabilized zirconia (YSZ), it is impractical to fabricate an entire resonant cavity from the HTS material for R_s measurements. Therefore, one method commonly adopted is to compare the quality factor (Q) of a metal cavity with and without a small superconducting sample enclosed. This perturbation procedure, ideally suited for measuring high R_s values, involves a careful and difficult determination of a rather small fractional difference between two large values of separately measured Q's because the HTS sample contributes only a negligibly small fraction of the total cavity loss. Other methods commonly in use are patterned superconducting stripline [9] or coplanar resonators [10].

The parallel-plate-resonator (PPR) technique developed by Taber [11] affords an ideal alternative to determine the surface impedance with high sensitivity. It is best suited for measuring R_s values ranging from 10 $\mu\Omega$ to 1 mΩ around 10 GHz. This method requires no lithographic patterning that may somewhat degrades the material quality. The current distribution over the tested films is quite uniform, making the R_s extraction simple and straightforward. Meanwhile, the frequency shift with temperature can be easily identified; hence the penetration depth of the superconducting samples can be inferred [8]. There are several disadvantages, however, with this technique. First, two identical films, both in dimensions and physical properties, are required in the measurement. Second, any metallic residue left over from processing on the back sides or the edges of the substrates can degrade the measured Q. Third, the resonance signal is sometimes difficult to detect because of difficulties in establishing the proper alignment to reach an optimum coupling between the coaxial probes and the resonator. In particular, the parallel-plate mode usually deviates from an ideal Lorentzian shape due to coupling between the resonator and the cavity enclosure, making it

Manuscript received October 19, 1995; revised February 15, 1996. This work was supported by the National Science Foundation under Grant NSF-DMR-91-20000, through the Science and Technology Center for Superconductivity under Grant DMR-91-20000.

The authors are with the Science and Technology Center for Superconductivity, Department of Electrical and Computer Engineering, University of Illinois, Urbana, IL 61801 USA

Publisher Item Identifier S 0018-9480(96)03788-X

difficult to determine the intrinsic resonance linewidth. This problem is carefully dealt with in the present work.

Because the PPR geometry is in analogy with a stripline configuration where the cavity chamber constitutes the ground plate and the superconducting films form the center strips, the observed cavity modes are associated with both the cavity chamber and the superconducting plates. When two modes (e.g., a resonator mode and a cavity mode) propagate in the chamber, the signal may not remain in phase and dispersion may occur due to different phase velocities for different modes [12], resulting in a considerable signal distortion when their resonant frequencies are close. Although this situation is not desired in practical measurements, it is not always possible to eliminate the undesired mode that falls near the other mode of interest. Therefore, it is necessary to establish an understanding of the coupling mechanism. In this paper, a systematic study of the frequency-dependent resonance spectra of the cavity and resonator is presented. We find that the unusual antiresonance features result from a phase interference of the wave functions between different modes and can be modeled with a theory of linearly coupled harmonic oscillators.

II. Theory

A. Field Distributions in a Parallel Plate Resonator

To understand how the PPR technique works, it is helpful to briefly discuss the electromagnetism of the PPR. The resonator presents open-circuited boundary conditions as illustrated in Fig. 1. Transverse electromagnetic modes can be excited between the superconducting plates to form standing waves. Because the separation (a dielectric spacer of typically $d =$ 10 to 50 μm) between the plates is much smaller than the film dimensions (1 cm $\times$ 1 cm) and the microwave wavelength ($\lambda \sim 1$ cm), three assumptions can be made. First, we can neglect the fringing fields. Second, the electromagnetic fields are essentially constant within the spacer along the normal (or z) direction. Third, the tangential components of the $\boldsymbol{E}$ field should vanish as required by the boundary conditions for perfectly conducting plates. The solution of the $\boldsymbol{E}$ field distribution is [13]

$$\boldsymbol{E} = \hat{z} E_0 \cos\frac{n\pi x}{a} \cos\frac{m\pi y}{b} \tag{1}$$

where a and b are the surface dimensions ($\sim$1 cm) of the resonator, n and m represent mode indices, and $\hat{z}$ is chosen normal to the sample surfaces so that the modes are named E_z or TM_{nm} modes. The magnetic field ($\boldsymbol{H}$) and surface current ($\boldsymbol{K}$) distributions can be obtained [12]:

$$\begin{cases} \boldsymbol{H} = \dfrac{j}{\omega\mu_0} \nabla \times \boldsymbol{E} = H_x\hat{\boldsymbol{x}} + H_y\hat{\boldsymbol{y}} \\ \boldsymbol{K} = \hat{\boldsymbol{z}} \times \boldsymbol{H} = K_x\hat{\boldsymbol{x}} + K_y\hat{\boldsymbol{y}} \end{cases} \tag{2}$$

where $\omega = 2\pi f$ is the angular frequency and μ_0 is the magnetic permeability of free space. Other terms in (2) are given by

$$\begin{cases} H_x = K_y = -j\dfrac{m\pi}{\mu_0\omega b} E_0 \cos\dfrac{n\pi x}{a} \sin\dfrac{m\pi y}{b}, \\ H_y = -K_x = j\dfrac{n\pi}{\mu_0\omega a} E_0 \sin\dfrac{n\pi x}{a} \cos\dfrac{m\pi y}{b}. \end{cases} \tag{3}$$

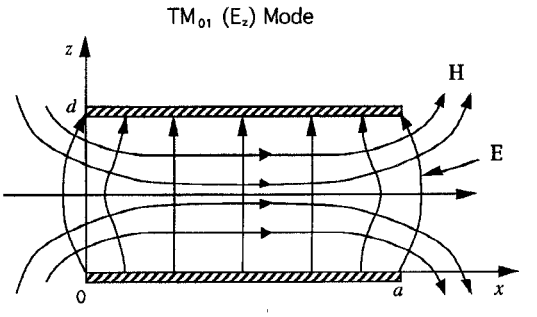

Fig. 1. Profile of the field lines for the TM_{01} mode of a parallel plate resonator. For visualization convenience, the distance, d, between the two plates has been greatly exaggerated. In reality, $d = 12.5$ μm, and $a = b = 1$ cm, suggesting that the edge effect is confined to a negligibly small fraction of the total area of the PPR.

Note both $\boldsymbol{H}$ and $\boldsymbol{K}$ have no components in the z direction. Equation (3) indicates that the tangential $\boldsymbol{H}$ components near the sample edges are vanishingly small, and that the components of the surface current normal to the edges vanish at the boundaries ($K_x = 0$ at $x = 0, a$; $K_y = 0$ at $y = 0, b$) as expected for open-circuited boundary conditions. In Fig. 1, the field lines for the TM_{01} mode are illustrated.

B. Determinations of Superconductor Parameters

On substitution of (1) into the Helmholtz wave equation, one can obtain the resonant frequency:

$$f_0 = \frac{v_p}{2}\sqrt{\left(\frac{n}{a}\right)^2 + \left(\frac{m}{b}\right)^2} \tag{4}$$

where $v_p = c/\sqrt{\epsilon}$ is the phase velocity in the medium with a relative dielectric constant ϵ between two plates. In our experiment, $\epsilon = 2.04$, $a = b = 1$ cm, giving a predicted $f_0 \approx 10.5$ GHz for the TM_{01} or TM_{10} mode. Note that degeneracy occurs for $a = b$.

In practice, a resonance always has a finite half-power width Δf due to microwave losses. When the PPR is housed in a small conductive chamber, the radiation loss due to field leakage out of the PPR increases linearly with the spacing d [11], [14]. In contrast, the dielectric loss is independent of d and the loss due to R_s of the conducting plates varies as $1/d$. Therefore, if d is small enough, the conductor loss becomes dominant and one can neglect the radiation and dielectric losses. In this case, the unloaded Q-factor of the PPR is given by [11]

$$\begin{aligned} Q &= \frac{f_0}{\Delta f} \\ &= \frac{\omega_0(W_E + W_M)}{P_c} \\ &= \frac{\pi\mu_0 f_0 d}{R_s} \end{aligned} \tag{5}$$

where W_E and W_M are the average electric and magnetic energies, respectively, stored in the resonator, and P_c is the average power lost in the resonator plates. Therefore, the surface resistance R_s can be determined directly from the 3-dB bandwidth Δf of the resonance peak. Note that the

determination of R_s is independent of the particular mode excited in the superconducting resonator.

The London penetration depth (λ_L) of the superconducting films can be determine from the resonant frequency. It is the change of λ_L that results in the frequency shift. In light of the nonzero value of λ_L, we must account for the effect of field penetration into the superconducting plates by replacing the dielectric constant ϵ of the medium by an effective value [15]

$$\epsilon_{\text{eff}} = \left(1 + \frac{2\lambda_L}{d} \coth \frac{t}{\lambda_L}\right)\epsilon \tag{6}$$

where t is the thickness of the superconducting films. Therefore, λ_L is related to the resonant frequency by

$$\frac{f_0(T)}{f_0(T_0)} = \sqrt{\frac{1 + \dfrac{2\lambda_L(T_0)}{d} \coth \dfrac{t}{\lambda_L(T_0)}}{1 + \dfrac{2\lambda_L(T)}{d} \coth \dfrac{t}{\lambda_L(T)}}} \tag{7}$$

where T_0 is an arbitrary temperature. Therefore, once $\lambda_L(T_0)$ is known, $\lambda_L(T)$ at any temperature can be determined by measuring the resonant frequency $f_0(T)$ and then inverting (7).

Finally, the complex conductivity σ can be obtained from the surface resistance R_s and the penetration depth λ_L according to

$$\begin{aligned} Z_s &= R_s + j\mu_0\omega_0\lambda_L \\ &= \sqrt{\frac{j\mu_0\omega_0}{\sigma}}. \end{aligned} \tag{8}$$

III. Experimental

A parallel plate resonator, shown in Fig. 2, was constructed using two unpatterned identical superconducting thin films grown on low loss $LaAlO_3$ (1 cm × 1 cm) wafers. A thin teflon dielectric spacer ($d = 12.5$ μm and $\epsilon = 2.04$) was sandwiched between the superconducting samples to form the PPR structure. The resonator was then positioned at the center of a cavity chamber machined from oxygen free high-conductivity (OFHC) copper. The cavity, a metallic shield meant to minimize the radiation loss, was polished and gold plated in order to reduce surface loss and prevent corrosion. Two nylon dielectric posts (one was spring loaded) were used to press the samples together, insuring that the samples are stationary during measurements and that there was no electrical contact between the resonator and the cavity enclosure.

The microwave signal was launched into and was measured at the output of the cavity/resonator assembly using two parallel, semirigid, 50-Ω coaxial cables that inserted through the top of the cavity. Both cables were connected to a Hewlett Packard 8510 microwave vector network analyzer for two-port scattering matrix measurements. Two micrometers were used to adjust independently the distances between the coaxial probes and the resonator to find an optimum coupling. The incident microwave power was chosen at 1 mW to avoid the high-power nonlinear effect [16]. Optimum coupling was obtained in the undercoupled regime so that the loaded and unloaded Q were essentially indistinguishable. Such condition usually occurs when the probe tips are within tenths of 1 mm from the top resonator edge positioned between the inner and outer conductors of the coaxial cables.

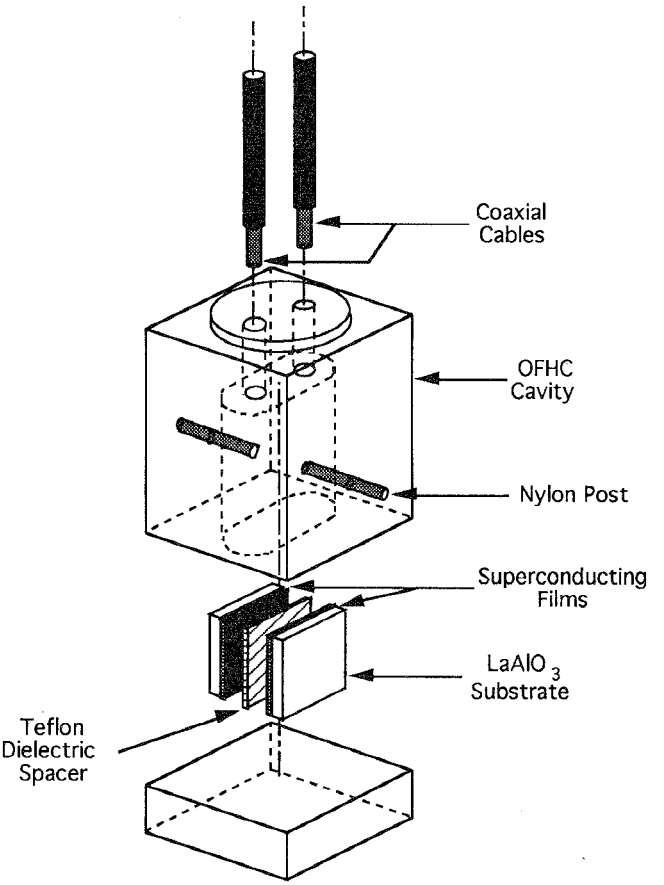

Fig. 2. Schematic of the parallel plate resonator and the cavity enclosure. A 12.5-μm-thick teflon spacer is sandwiched between two (1 cm × 1 cm) superconducting samples to form the PPR. The microwave swept signal is sent through one port and collected from the other port of the coaxial cables using a HP 8510 microwave vector network analyzer.

Cryogenic measurements were performed with the setup placed in a liquid helium dewar. A DT-470 silicon diode temperature sensor and a heater resistor were anchored on the exterior surface of the copper cavity. Both the sensor and the heater were connected to a LakeShore DRC-91CA temperature controller so that temperature variation could be monitored and controlled automatically. In addition, there was an intake in the top of the cavity through which helium gas could be sent to purge the test chamber during the cooling and warming processes. This is an important step to avoid water condensation on the inner cavity walls, the probe tips, and the sample surfaces. The frequency-dependent S-parameter data were collected over a large temperature range between 6 K and T_c (~90 K) of the $YBa_2Cu_3O_7$ films.

IV. Results and Discussion

Because the cavity chamber is not appreciably larger than the PPR, one expects that the test chamber modes would fall close to the PPR modes. The resonator modes are governed by the intrinsic responses of the superconducting samples,

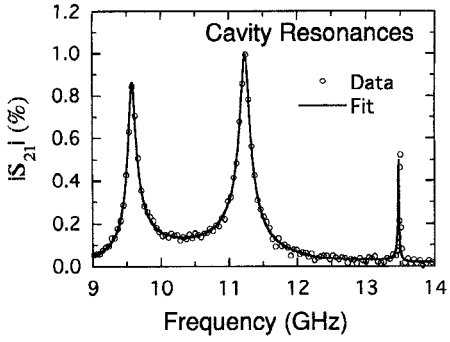

Fig. 3. Experimental transmission coefficient $|S_{21}|$ of the test chamber (open circles on every 5th data point), showing three resonance peaks that can be fit well (solid line) by the Lorentz model using an extended form of (12) with three oscillators.

whereas the cavity modes are in principle extrinsic to sample properties. However, the presence and the location of the PPR will modify the resonant frequencies of the cavity modes because of the stripline-like geometry.

A. Resonance of Empty Cavity

To identify the extraneous chamber modes, the cavity chamber *without* a resonator inside has been tested. As illustrated in Fig. 3, three modes in the range of 9–14 GHz have been observed. These cavity resonance peaks can be fit well by a Lorentz oscillator model as shown in the figure. Given the dimensions of a cavity, one can in principle calculate the resonant frequencies. However, the exact solution for our cavity chamber is not simplistic because the boundary involves a mixture of rectangular and circular geometry. Nonetheless, given the chamber size ($\sim$1 cm), we can infer that the lower modes will fall around 10 GHz. Therefore, the observed three resonances in Fig. 3 are attributed to the cavity modes. This argument is supported by the observation of a clear frequency shift when we change the cavity volume. Interestingly, all observed cavity modes shift to lower frequencies as the test probes move forward in the cavity, suggesting that the resonant frequencies are strongly modulated by the capacitance between the test probes and the cavity. An electric or capacitive coupling occurs for open-ended probe configuration [17], the case here. (For shorted loops, the coupling is magnetic or inductive.)

We note that the first two modes have a quite poor Q-factor, possibly due to some spurious coupling to the test probes. Because the test chamber designed for this experiment is not a completely enclosed single cavity (see Fig. 2), additional losses can be induced by other sources such as the stainless-steel outer conductor of the inserted feed cables, the holes used for the nylon posts and helium gas intake, the air gaps around the bottom lid, and some leakage between the input and output couplers [11]. Nevertheless, since the field lines for the excited PPR mode are mostly confined within the resonator plates, the external sources mentioned above would not directly contribute to the PPR loss. Therefore, this problem does not affect the analysis of interaction between the PPR and the overall test chamber, the primary interest of the present work.

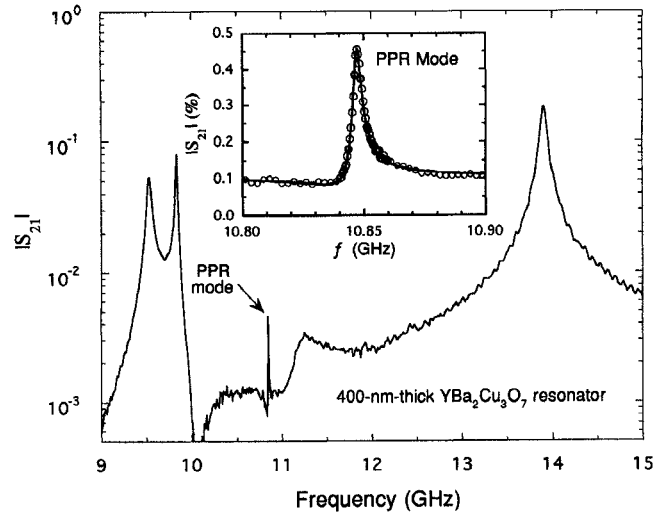

Fig. 4. Measured microwave resonance for a 400-nm-thick $YBa_2Cu_3O_7$ thin-film PPR placed in the cavity chamber at $T \ll T_c$. The resonator mode at 10.848 GHz lies on a broad background of the external cavity modes. Inset: Expanded view of the PPR mode where the peak is asymmetric. Data are plotted in open circles and a model fit is shown in solid line.

B. Resonance of Parallel Plate Resonator with the Cavity Enclosure

It is expected that the cavity modes may influence the line shape of the lowest PPR mode located in the same frequency regime. Fig. 4 shows a typical microwave response of a $YBa_2Cu_3O_7$ parallel plate resonator placed inside the cavity at a temperature much below T_c. The $YBa_2Cu_3O_7$ films have a $T_c = 90$ K and are 400-nm thick grown on 0.5-mm $LaAlO_3$ substrates by *in situ* off-axis sputtering.

Several strong modes are observed in the 9–15 GHz range, and a weak but much sharper peak near 11 GHz stands out. The frequency of this sharp peak—identified as a superconductive PPR mode—agrees well with the theoretical value (10.5 GHz) predicted by (4) for the TM_{01} or TM_{10} mode. Other modes are attributed to the cavity enclosure. Several convincing tests have been performed to confirm such mode identifications. First, we find that the sharp 11-GHz feature disappears while others do not after removing the teflon dielectric spacer, leaving the two HTS films in direct electrical contact. Second, with the teflon spacer in position, we observe that the 11-GHz mode clearly shifts toward lower frequency and broadens rapidly with increasing temperature, whereas that the other modes essentially remain unchanged in resonant frequencies or line widths as T is varied. For the PPR mode, the absorptive broadening results from an increase in the number of thermally excited quasiparticles across the superconducting gap, causing a rapid enhancement in R_s. The inductive frequency downshift, described by (7), results from an increased London penetration depth. Third, all cavity modes exhibit a clear frequency shift (as happened in the empty cavity described above) when the test probe tips are moved slightly. The resonator mode, however, remains in position. Finally, the resonator mode gradually disappears as the temperature approaches T_c. In contrast, the cavity modes (or stripline modes) do not change until $T \lesssim T_c$ when the loss of the

normal-state $YBa_2Cu_3O_7$ plates (center strips) dominates over that of the cavity walls (stripline ground).

The inset of Fig. 4 shows an expanded view of the resonator peak (along with a model-fit curve to be discussed below). A conventional 3-dB (half-power) estimate gives a linewidth $\Delta f = 3.95$ MHz. However, as seen in the figure, a considerable background is present and should be subtracted to avoid an overestimate of Δf or R_s. Furthermore, the line shape of the PPR is asymmetric and distorted due to coupling between the PPR and its neighbor cavity mode(s). To extract the intrinsic Q of the resonator, a least-square fit with a proper model must be employed.

C. Mode Coupling and Antiresonance

We find that a symmetric resonance or a simple, Lorentzian-like line shape of the PPR mode can be obtained only if the resonance is located near the minimum between two extraneous cavity modes, provided the background level of this minimum is very small. This condition sometimes can be fulfilled after careful alignment but it is usually difficult to achieve. On the other hand, if the PPR mode occurs near the maximum of a cavity mode (easily obtained by adjusting the coupling probes or changing the temperature), a considerable distortion or even an antiresonant feature will be observed.

Fig. 5 plots the experimental data (dashed lines) for another pair of $YBa_2Cu_3O_7$ films grown on 0.5-nm thick $LaAlO_3$ substrates, showing the strong coupling effect and the antiresonance features. The films have dimensions of 9.8 mm × 9.8 mm × 200 nm with $T_c = 85$ K. Starting at $T = 72$ K, the PPR mode manifests itself by a sharp *antiresonance* notch near 11 GHz. Three other broad peaks shown in the figure are cavity modes. (The solid lines in Fig. 5 are model fits to be discussed next.) Note that the positions of the cavity (or stripline) modes differ from those shown in Fig. 4 because of different sample sizes and locations inside the test chamber. As the temperature is increased, this minimum shifts to a lower frequency and it grows deeper as it moves closer to the peak of a cavity mode at 10.5 GHz, indicating an increased coupling between these two modes.

Obviously, one cannot find the resonator Q-factor simply from the 3-dB bandwidth in Fig. 5 because this interesting feature certainly cannot be described by a model of independent oscillators. To extract the intrinsic resonator Q, we have used two classical approaches to fit the experimental data. One is a generalized Lorentz model in which oscillators have different initial phases. The other is a more rigorous model in which two oscillators interact through a linear coupling spring constant. It turns out that these approaches can satisfactorily fit our data. In particular, the former is good enough for weak coupling and the latter is more general for both weak and strong couplings. This analysis is presented below.

V. Coupling Model Analysis

A. Phase Interference between Two Damped Electric Fields

The observed antiresonance may result from interference between two out-of-phase electric fields of the coupled modes.

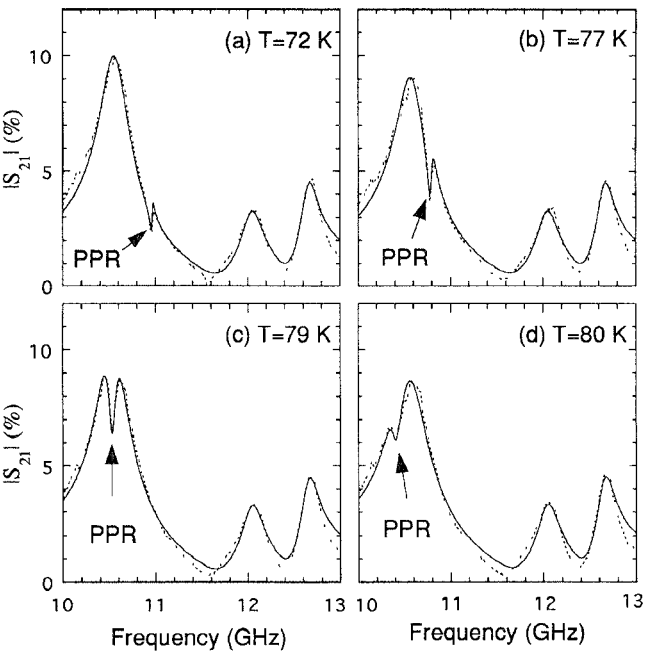

Fig. 5 Measured spectra for a 200-nm-thick $YBa_2Cu_3O_7$ resonator at four selected temperatures near T_c, showing an *antiresonance* feature around 10.5 GHz due to mode coupling. In contrast to the strong T-dependence of the notch-like PPR mode, the cavity modes remain nearly temperature independent. The dashed lines are measured data, and the solid lines are calculated using a linearly-coupled oscillator model given by (21). (See Table I for fitting parameters.).

When their eigenfrequencies are close and one has a much narrower resonance than the other, strong destructive interference may occur, causing a sharp minimum on the broad peak of the other mode. When their eigenfrequencies are far apart, however, normal resonance would recover since the overlapping or interference effect is greatly reduced. To see this effect, we should first briefly review the simplest damped harmonic oscillator model.

The finite width of an excited mode is caused by energy dissipation in the cavity (or resonator) walls and in the dielectric filling within the enclosure. In the time domain, the energy stored in the enclosure decays exponentially $U(t) = U_0 e^{-\Gamma t}$, where Γ is the damping rate. The damped electric field is

$$\boldsymbol{E}(t) = \boldsymbol{E}_0 e^{-\Gamma t/2} e^{j\omega_0 t} \tag{9}$$

where ω_0 is the angular resonant frequency, $\boldsymbol{E}_0$ is the initial amplitude at $t = 0$ and is in general complex, ($\boldsymbol{E}_0 = |\boldsymbol{E}_0| e^{j\phi_0}$). One can simplify (9) to $\boldsymbol{E}(t) = \boldsymbol{E}_0 e^{j\omega_0' t}$ by introducing a complex resonant frequency ($\omega_0' = \omega_0 + j\Gamma/2$) to account for the dissipation effect.

The frequency-domain $\boldsymbol{E}$-field is the Fourier transformation of (9)

$$\begin{aligned} \boldsymbol{E}(\omega) &= \int_0^\infty \boldsymbol{E}(t) e^{-j\omega t}\, dt \\ &= \frac{j\boldsymbol{E}_0}{\omega_0 - \omega + \dfrac{j\Gamma}{2}}. \end{aligned} \tag{10}$$

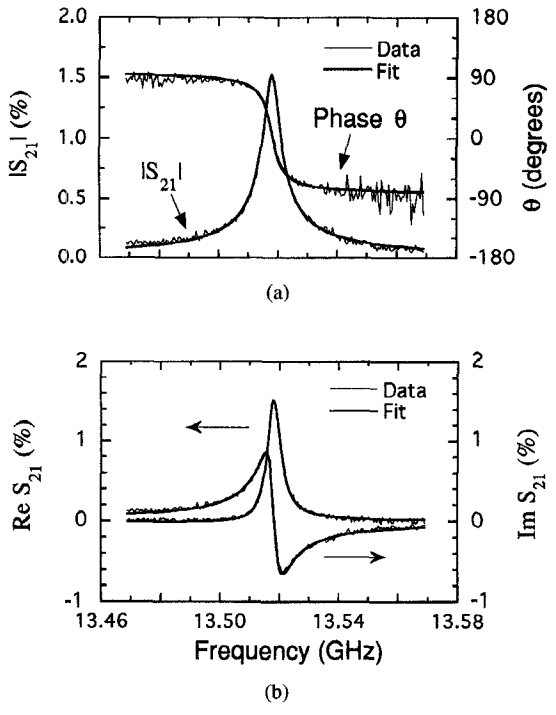

Fig. 6. (a) The amplitude and phase and (b) the real and imaginary parts of S_{21} for a single cavity mode. Experimental data (thin lines) are compared with fits (thick curves) using a single uncoupled oscillator model given by (12). The fitting parameters are $S = 0.0152$, $f_0 = 13.518$ GHz, $\gamma = 5.50$ MHz, and $\phi_0 = 7.5°$.

Equation (10) describes a damped harmonic oscillator that has a Lorentzian line shape with a 3-dB bandwidth Γ. The Q factor is $Q = \omega_0/\Gamma$ and the phase is

$$\theta = \phi_0 + \arctan\left(\frac{\omega_0 - \omega}{\frac{\Gamma}{2}}\right). \tag{11}$$

Assuming the transmission coefficient S_{21} have the Lorentzian form as (10)

$$S_{21} = \frac{jSe^{j\phi_0}\frac{\gamma}{2}}{f_0 - f + \frac{j\gamma}{2}} \tag{12}$$

where S is the normalized oscillator strength or the peak value of $|S_{21}|$ at $f = f_0$ with $f = \omega/2\pi$ and $\gamma = \Gamma/2\pi$. Excellent fits to the experimental data are obtained (see Fig. 6) using (12) for an empty-cavity mode, indicating that an uncoupled microwave resonance follows the behavior of a damped harmonic oscillator.

We now consider a weak and sharp *resonator* mode $\boldsymbol{E}_r$ falling near the center frequency of a broad *cavity* mode $\boldsymbol{E}_c$, the case in our experiment. The total electric field in the time domain is

$$\begin{aligned}\boldsymbol{E}(t) = &|\boldsymbol{E}_c|e^{-\Gamma_c t/2}e^{j(\omega_c t+\phi_c)} \\ &+ |\boldsymbol{E}_r|e^{-\Gamma_r t/2}e^{j(\omega_r t+\phi_r)}.\end{aligned} \tag{13}$$

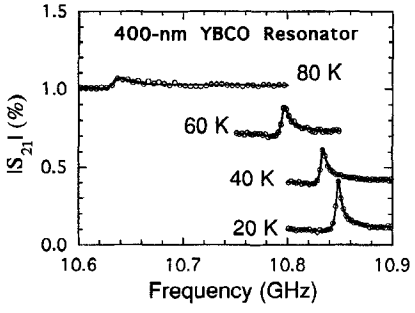

Fig. 7. Resonance for the 400-nm $YBa_2Cu_3O_7$ resonator at four selected temperatures, showing the Fano-type asymmetric distortion of the resonance. The peak shifts to lower frequency and the line broadens with decreasing temperature. For clarity, the curves for 40, 60, and 80 K are shifted up by 0.3, 0.6, and 0.9%, respectively. Raw data are plotted in open circles (every 5th data point) and solid lines are least-square fits using (14).

The Fourier transformation of (13) gives the frequency-domain response

$$|\boldsymbol{E}(\omega)| = \left|\frac{|\boldsymbol{E}_c|}{\omega_c - \omega + \frac{j\Gamma_c}{2}} + \frac{|\boldsymbol{E}_r|e^{j\phi}}{\omega_r - \omega + \frac{j\Gamma_r}{2}}\right| \tag{14}$$

where $\phi = \phi_r - \phi_c$ is the initial phase difference between two modes. It is this phase factor that causes a resonance distortion. We find that, for *weak* mode coupling, the expression (14) can describe and fit satisfactorily our spectra as demonstrated in Fig. 7, in which the line broadening and frequency shift with temperature for the PPR mode is also illustrated.

B. Coupled Harmonic Oscillators

We now propose another coupling model that can better explain the observed strong asymmetric and antiresonant features. This model assumes a linear coupling between harmonic oscillators. Similar antiresonance behavior arising from electron-phonon interaction for high-dielectric-constant materials ($BaTiO_3$, $SrTiO_3$, and $KTaO_3$) have been observed by Spizer *et al.* [18] and explained by Barker and Hopfield [19]. Rice [20] pointed out that a linear coupling of charge carriers to symmetric phonons could lead to a notch-like structure in the conductivity at the phonon frequencies. Timusk and Tanner [21] have reported that the coupling between a phonon and a broad electronic background could give a notch in the infrared conductivity of oxide superconductors. However, such effect has not been reported for microwave resonance.

To understand the observed antiresonance in microwave PPR, we model the response function and describe the equations of motion by two damped and linearly coupled harmonic oscillators:

$$\begin{cases} m_1\dfrac{d^2x_1}{dt^2} = -k_1x_1 - m_1\Gamma_1\dfrac{dx_1}{dt} \\ \quad -g(x_1 - x_2) + q_1E, \\ m_2\dfrac{d^2x_2}{dt^2} = -k_2x_2 - m_2\Gamma_2\dfrac{dx_2}{dt} \\ \quad -g(x_2 - x_1) + q_2E \end{cases} \tag{15}$$

where m_i, x_i, k_i, Γ_i, and $q_i (i = 1, 2)$ are the mass, displacement, force constant, damping rate, and charge, respectively,

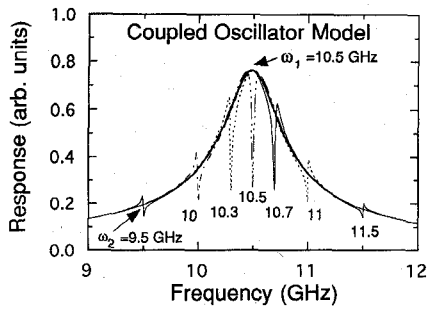

Fig. 8. Model calculation for the magnitude of the response function using (19) for two linearly-coupled harmonic oscillators, showing the *antiresonance* structures of the narrow mode located at $\omega_2/2\pi = 9.5, 10, 10.3, 10.5, 10.7, 11$, and 11.5 GHz with $\omega_g/2\pi = 1$ GHz and $\Gamma_2/2\pi = 10$ MHz. The broad peak located at $\omega_1/2\pi = 10.5$ GHz has $\omega_{p1}/2\pi = 2$ GHz and $\Gamma_1/2\pi = 0.5$ GHz.

of the ith oscillator; E is the driving electric field. The linear coupling constant g describes the coupling strength between two oscillators.

Assuming the local field has a time dependence of $e^{j\omega t}$, one obtains

$$\begin{cases} m_1(\omega_1^2 - \omega^2 + j\Gamma_1\omega)x_1 = gx_2 + q_1E \\ m_2(\omega_2^2 - \omega^2 + j\Gamma_2\omega)x_2 = gx_1 + q_2E \end{cases} \tag{16}$$

where $\omega_i = \sqrt{(k_i + g)/m_i}\,(i = 1, 2)$. Solving (16), we find

$$x_1 = \left(\frac{1 + G_2 \dfrac{q_2}{q_1}\sqrt{\dfrac{m_1}{m_2}}}{\omega_1^2 - \omega^2 + j\omega\Gamma_1 - \omega_g^2 G_2} \right) \frac{q_1}{m_1} E \tag{17}$$

where

$$G_2 = \frac{\omega_g^2}{\omega_2^2 - \omega^2 + j\omega\Gamma_2} \tag{18}$$

is Green's function or propagator for oscillator 2 with $\omega_g^2 = g/\sqrt{m_1 m_2}$ being the coupling frequency. By symmetry, the expression of x_2 is given by interchanging the indices in (17) and (18). For $x_2 \ll x_1$ and weak coupling $G_2 \ll 1$, we can treat mode 2 as a small perturbation of mode 1, as the case in our experiment. The second term of the numerator in (17) can then be neglected. Given the induced dipole moment $p_1 = q_1 x_1$ and supposing the dipole density is N_1, we obtain the response function of the system

$$\begin{aligned} \mathcal{R}(\omega) &= \frac{N_1 p_1}{\epsilon_0 E} \\ &= \frac{\omega_{p1}^2}{\omega_1^2 - \omega^2 + j\omega\Gamma_1 - \omega_g^2 G_2} \end{aligned} \tag{19}$$

where $\omega_{p1}^2 = N_1 q_1^2/\epsilon_0 m_1$ is the oscillator strength of mode 1. Fig. 8 illustrates the calculated results using (19) for two linearly coupled oscillators with $\Gamma_2 \ll \Gamma_1$. This model predicts a strong antiresonance as ω_2 approaches ω_1.

It should be pointed out that if mode 2 is far away from the center frequency of mode 1 such that $|\omega_2 - \omega_1| \gg \Gamma_1$, the tail level of mode 1 at ω_2 is then no longer much larger than the magnitude of mode 2, but the opposite is true ($x_2 \gg x_1$ at ω_2). In a small range around ω_2, we should treat the tail of mode 1 as a small perturbation of mode 2. In this case, x_2 dominates over x_1 and the response function would be

$$\mathcal{R}(\omega) = \frac{\omega_{p2}^2}{\omega_2^2 - \omega^2 + j\omega\Gamma_2} \tag{20}$$

where the G_1 term is dropped from (20) because it is vanishingly small near ω_2. The expression of (20) recovers the form of (10) or (12) since $\omega_2^2 - \omega^2 \approx 2\omega(\omega_2 - \omega)$ for $\omega \approx \omega_2$. In other words, the symmetric Lorentzian line shape is recovered because the two oscillators are decoupled.

To apply this model to fit our spectra with more than one cavity mode, we generalize (19) into

$$\begin{aligned} \mathcal{R}(\omega) = &\frac{\omega_{p1}^2}{\omega_1^2 - \omega^2 + j\omega\Gamma_1 - \omega_g^2 G_2} \\ &+ \sum_{i>2} \frac{\omega_{pi}^2}{\omega_i^2 - \omega^2 + j\omega\Gamma_i}. \end{aligned} \tag{21}$$

Taking the S_{21} as a response function in the form of (21), we compare the experimental data with the model fitting as shown in Fig. 5. The excellent fits strongly support the validity of this coupling model. The fitting parameters are summarized in Table I. We can see from the table that, in contrast to the PPR ($i = 2$) mode, the parameters for the cavity modes indexed $i = 1, 3, 4$ are essentially temperature independent.

We note that the bandwidths (Δf_0 or $\Gamma/2\pi$) of the PPR mode for these 200-nm films are broader than those for the 400-nm $YBa_2Cu_3O_7$ films (Fig. 7). The difference is attributed to the fact that the former samples have smaller thickness ($d \lesssim \lambda_L$); thus radiation leakage through the films becomes significant. In addition, there are many silver residues left over on the backsides and the edges of the former films, causing additional microwave losses. The latter samples, in contrast, appear to be better quality; they are thicker, cleaner, and have higher T_c. Nevertheless, the major interest of this paper is coupling analysis of the antiresonance features; thus sample quality is unimportant.

The accuracy of our model analysis has been further tested by fitting the spectra measured with the PPR enclosed in another differently-shaped cavity. (Besides, the geometry is rotated by 90° about the axis through the nylon posts compared to the one shown in Fig. 2.) Although the observed cavity resonance spectra exhibit quite a noticeable change, the coincidence of the fitted PPR parameters out of these two measurements is usually within 7%. For illustrative purpose, Fig. 9 demonstrates the resonant frequencies and Q values obtained by model fitting to the 400-nm-thick $YBa_2Cu_3O_7$ films, along with the calculated complex surface impedance $Z_s = R_s + jX_s$. The microwave loss of HTS is two orders of magnitude smaller than that of copper at 10 GHz and such advantage persists up to ~200 GHz [22]. All the extracted results, including the microwave conductivity, London penetration depth, and the quasiparticle scattering rate are in reasonable agreement with that reported in literature. The physical properties for our $YBa_2Cu_3O_7$ films resulting from the present analysis can be found elsewhere [8].

TABLE I
FITTING PARAMETERS OBTAINED BY USING A LINEARLY-COUPLED OSCILLATOR MODEL FOR A 200-NM-THICK $YBa_2Cu_3O_7$ SUPERCONDUCTING RESONATOR ENCLOSED IN A CAVITY (SEE THE CURVE FITTING IN FIG. 5)

T (K)	Osc. # i	$\omega_i/2\pi$ (GHz)	$\omega_{pi}/2\pi$ (GHz)	$\Gamma_i/2\pi$ (GHz)
72	1	10.565	0.590	0.332
	2	10.962	0.950	0.0185
	3	12.040	0.300	0.249
	4	12.650	0.317	0.200
77	1	10.585	0.583	0.355
	2	10.786	1.030	0.0365
	3	12.040	0.300	0.249
	4	12.650	0.317	0.200
79	1	10.540	0.602	0.353
	2	10.530	1.097	0.0680
	3	12.040	0.300	0.249
	4	12.650	0.317	0.200
80	1	10.550	0.615	0.405
	2	10.400	1.092	0.0997
	3	12.040	0.300	0.249
	4	12.650	0.317	0.200

Oscillator $i = 2$ represents the PPR mode with $\omega_g = \omega_{p2}$, and $i = 1,3,4$ the cavity modes.

Finally, we want to point out that the two descriptions of (14) and (19) are not totally irrelative or equally good. For weak coupling, the last term $(\omega_g^2 G_2)$ of the denominator in (19) is small. It is straightforward to show that the first order Taylor series expansion of (19) gives an expression similar to (14). The phase coupling model or (14) is simpler and we find it good enough in fitting spectra in which the eigenvalues of two modes are not too close, regardless of the relative strengths or widths of the individual modes (see, for examples, Figs. 3 and 4). In other words, it works well for weak coupling but not as well in the strong antiresonance regime because the model is too simple to describe this complicated strong interference effect. In contrast, the linear coupling model or (19) works in both weak and strong coupling regimes, provided the normal mode considered has much smaller amplitude than the nearest one it couples (see Fig. 5). The method, however, breaks down when the coupled modes have nearly equal strengths and damping widths.

VI. CONCLUSION

The coupling effect between a superconducting parallel plate resonator and a surrounding cavity has been carefully analyzed. The microwave response of the system can be described well by an independent Lorentz oscillator model only if the resonance modes are well separated from one another. Strong interaction and antiresonance can occur when the eigenfrequencies of the cavity modes fall close to the parallel plate resonator mode. This characteristics may have possible applications in microwave devices when an antiresonance type of signal is desired. The observed behavior can be explained by a phase coherence and can be well described by a linearly-coupled oscillator model. This analysis provides an important insight in understanding the damping processes and the interaction between the microwave normal modes. Therefore, it provides a method to extract the intrinsic Q out of the "distorted" resonance structure of the parallel plate resonator.

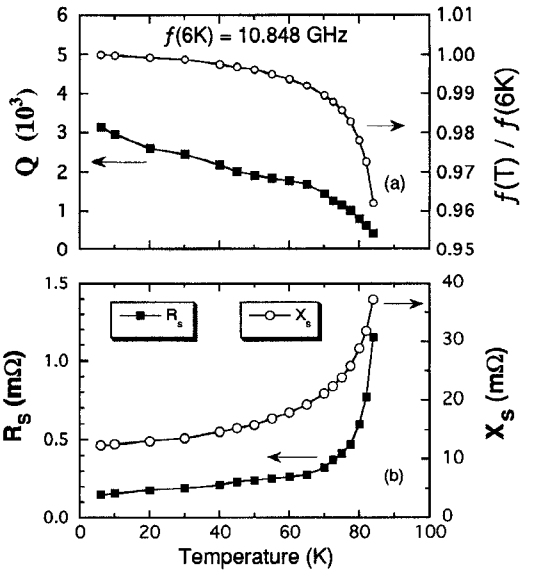

Fig. 9. (a) The measured Q factor and normalized resonant frequency obtained by model fit to the $|S_{21}|$ spectra of a 400-nm-thick $YBa_2Cu_3O_7$ resonator. (b) The real (R_s) and imaginary (X_s) parts of the surface impedance Z_s at 10 GHz. (The lines are guides to the eye.)

ACKNOWLEDGMENT

The authors would like to thank R. C. Taber, C. Wilker, M. B. Salamon, and D. B. Tanner for helpful discussions.

REFERENCES

[1] F. J. Winter and J. J. Taub, "High dielectric constant stripline band pass filters," *IEEE Trans. Microwave Theory Tech.*, vol. 39, p. 2182, 1991.
[2] G. L. Hey-Shipton, "Microwave applications of high-T_c superconductivity," in *Wescon Conf. Record,* Nov. 1992, p. 424.
[3] D. G. Swanson, R. Forse, and B. J. Nilsson, "A 10 GHz thin film lumped element high-T_c superconductor filter," in *IEEE MTT-S Symp. Dig.,* Albuquerque, NM, June 1992, p. 1191.
[4] R. B. Hammond, G. L. Hey-Shipton, and G. L. Matthaei, "Designing with superconductors," *IEEE Spectrum,* p. 34, Apr. 1993.
[5] A. Davidson, J. Talvacchio, M. G. Forrester, and J. R. Gavaler, "High-T_c materials expand superconductive circuit applications," *Microwaves & RF,* vol. 33, p. 140, Apr. 1994.
[6] M. Feng, F. Gao, Z. Zhou, J. Kruse, M. Heins, J. Wang, S. Remillard, R. Lithgow, M. Scharen, A. Cardona, and R. Forse, "High temperature superconducting resonators and switches: Design, fabrication, and characterization," *IEEE Trans. Microwave Theory Tech.*, to be published.

[7] G. B. Lubkin, "Applications of high-temperature superconductors approach the marketplace," *Phys. Today*, vol. 3, p. 20, 1995.
[8] F. Gao, J. W. Kruse, C. E. Platt, M. Feng, and M. V. Klein, "Microwave surface impedance at 10 GHz and quasiparticle scattering in $YBa_2Cu_3O_7$ films," *Appl. Phys. Lett.*, vol. 63, p. 2274, 1993.
[9] D. E. Oates, A. C. Anderson, D. M. Sheen, and S. M. Ali, "Stripline resonator measurement of Z_s versus H_{rf} in $YBa_2Cu_3O_7$ thin films," *IEEE Trans. Microwave Theory Tech.*, vol. 39, p. 1522, 1991.
[10] A. Porch, M. J. Lancaster, and R. G. Humphreys, "The coplanar resonator technique for determining the surface impedance of $YBa_2Cu_3O_7$ thin films," *IEEE Trans. Microwave Theory Tech.*, vol. 43, p. 306, 1995.
[11] R. C. Taber, "A parallel plate resonator technique for microwave loss measurements on superconductors," *Rev. Sci. Instrum.*, vol. 61, p. 2200, 1990.
[12] M. V. Klein, *Optics*. New York: Wiley, 1970.
[13] I. J. Bahl and P. Bhartia, *Microstrip Antennas*. Dedham, MA: Artech House, 1980.
[14] A. Y. Basovich, R. K. Belov, V. A. Markelov, L. A. Mazo, S. A. Pavlov, V. V. Talanov, and A. V. Varganov, "Parallel-plate resonator of variable spacer thickness for accurate measurements of surface impedance of high-T_c superconductive films," *J. Superconduct.*, vol. 5, p. 497, 1992.
[15] R. L. Kautz, "Picosecond pulses on superconducting striplines," *J. Appl. Phys.*, vol. 49, p. 308, 1978.
[16] F. Gao, Z. Zhou, M. Feng, M. Scharen, A. Cardona, and R. Forse, "Hysteresis effect in microwave power transmission of high temperature superconducting coplanar transmission lines," *Appl. Phys. Lett.*, vol. 67, p. 2229, 1995.
[17] D. M. Pozar, *Microwave Engineering*. New York: Addison-Wesley, 1990.
[18] W. G. Spitzer, R. C. Miller, D. A. Kleinman, and L. E. Howarth, "Infrared measurements on high dielectric constant materials BaTiO, SrTiO, and KTaO," *Phys. Rev.*, vol. 126, p. 1710, 1962.
[19] A. S. Barker and J. J. Hopfield, "Coupled-optical-phononmode theory of the infrared dispersion in BaTiO, SrTiO, and KTaO," *Phys. Rev.*, vol. 135, p. 1732, 1964.
[20] M. J. Rice, "Organic linear conductors as systems for the study of electron-phonon interactions in the organic solid state," *Phys. Rev. Lett.*, vol. 37, p. 36, 1976.
[21] T. Timusk and D. B. Tanner, "Evidence for strong bound-electron-phonon interaction at 52 meV in $YBa_2Cu_3O_7$," *Physica C*, vol. 169, p. 425, 1990.
[22] F. Gao, J. F. Whitaker, C. Uher, S. Y. Hou, and J. M. Phillips, "High-frequency surface impedance and penetration depth of $YBa_2Cu_3O_7$ films: Coherent time-domain spectroscopy method," *IEEE Trans. Appl. Superconduct.* vol. 5, p. 1970, 1995.

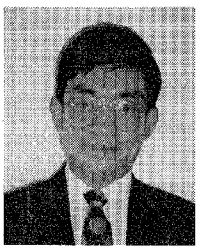

Feng Gao (M'93) received the B.Sc. degree from the Jinan University, China, in 1982, the M.S. degree in physics from the California State University at Northridge in 1986, and the Ph.D. degree in physics from the University of Florida, Gainesville, in 1992.

From 1992 to 1995, he worked as a Postdoctoral Research Associate jointly with the NSF Science and Technology Center for Superconductivity, Department of Electrical and Computer Engineering, Department of Physics, Materials Research Laboratory at the University of Illinois at Urbana-Champaign, and the Ultrafast Optical Science Laboratory within the Electrical Engineering and Computer Science Department at the University of Michigan, Ann Arbor. He has been involved in spectroscopy analysis of superconducting thin films over the frequency range from microwave, millimeter-wave, infrared, visible through ultraviolet. His interests include characterization of superconductor and semiconductor materials, circuit design, modeling, and high-speed MMIC device applications, analysis of resonators, transmission lines, and filters. He has authored or coauthored more than 40 journal and conference papers. In October 1995, he became a Senior Electrical Engineer with M/A-COM, doing microwave research on semiconductor integrated-circuit devices such as MESFET, LNA, and power amplifiers for wireless communication applications.

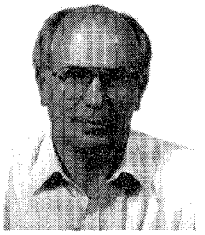

M. V. Klein (M'83–SM'83) was born in Cleveland, OH, in 1933. He received the B.S. degree in physics from Northwestern University, Evanston, IL, in 1954, and the Ph.D. degree in physics from Cornell University, Ithaca, NY, in 1961.

After spending a year as a National Science Foundation Fellow in Stuttgart, West Germany, he took a position as Assistant Professor at the University of Illinois at Urbana-Champaign, in 1962. He is currently a Professor of Physics and Director of the Science and Technology Center for Superconductivity at Illinois. His current research interests include optical properties of superconductors with emphasis on Raman scattering from electronic excitations. He is the author of more than 100 scientific articles, several review articles, and the textbook *Optics*, with T. L. Furtak (New York: Wiley, 1986).

Dr. Klein is a Fellow of the American Physics Society and the AAAS and a member of the Materials Research Society.

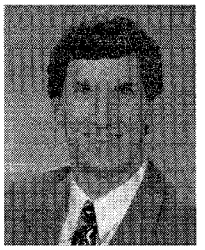

Jay Kruse (S'91–M'96) was born in Omaha, NE, in 1968. He received the B.S. degree in electrical engineering from Iowa State University, Ames, in 1990. He received the M.S. degree in 1992 and the Ph.D. degree in 1996 in the area of millimeter-wave circuit design and device characterization.

In 1991, he joined the High Speed Integrated Circuits Group at the University of Illinois at Urbana-Champaign. He is currently with Watkins–Johnson, Palo Alto, CA. His research interests include coplanar microwave and millimeter-wave circuit design for commercial communication systems, temperature dependent device characterization, and superconducting passive components.

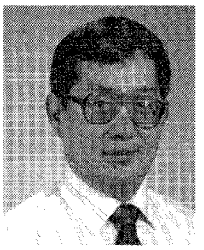

Milton Feng (M'82–SM'82–F'92) was born in Taiwan, China, on July 21, 1950. He received the B.S. degree in electrical engineering from Columbia University, New York, NY, in 1973, and the M.S. and Ph.D. degrees in electrical engineering from the University of Illinois, Urbana, in 1976 and 1979, respectively.

From 1979 to 1983, as Section Head of the material and device group at Torrance Research Center, Hughes Aircraft Company, Torrance, CA, he was in charge of ion implantation, $AsCl_3$ VPE, MOCVD, and MBE technology. In 1983, he developed an ion-implanted low-noise and power MESFET which resulted in the first demonstration of 60-GHz GaAs amplifiers. In 1984, he joined Ford Microelectronics, Inc., Colorado Springs, CO. He managed the advanced digital integrated circuit development program in 1 kbyte SRAM and 500 gate array. Later, he was the director of advanced development and fabrication on both digital and microwave/millimeter-wave development programs and manufacturing technology. In 1990, along with a coauthor, he demonstrated excellent power and low noise MESFET performance at 60 GHz, oscillator MESFET performance at 92 GHz to demonstrate integratable millimeter-wave IC, and ultrahigh-speed digital IC by ion-implantation MESFET technology. In 1990, he verified for the first time that 2DEG is not required for high-frequency and high-speed device performance due to the submicrometer FET dominated by high-field velocity rather than low-field mobility. Since 1991, he has been a Professor of Electrical and Computer Engineering and a member of the faculty of the Center for Compound Semiconductor Microelectronics at the University of Illinois, Urbana. His research interests include ion-implantation technology in III–V technology, optoelectronics IC's, ultrahigh-speed analog-digital HBT IC's, and microwave/millimeter-wave IC's on material, device, processing, design, and testing.

Dr. Feng received the Ford Aerospace Corporate Technology Outstanding Principal Investigator Award in 1989 for his contribution of advancing ion implantation GaAs and InGaAs MESFET into a manufacturable millimeter-wave IC with device $F_t > 100$ GHz and $f_{max} > 100$ GHz. He received the Beckman Research Award in 1994.